Arabian Journal of Chemistry (2018) **11**, 34–47

King Saud University

Arabian Journal of Chemistry

www.ksu.edu.sa
www.sciencedirect.com

ORIGINAL ARTICLE

Photocatalytic degradation of 1,2-dichlorobenzene using immobilized $TiO_2/SnO_2/WO_3$ photocatalyst under visible light: Application of response surface methodology

Renugambaal Nadarajan, Wan Azelee Wan Abu Bakar *, Rusmidah Ali, Razali Ismail

Department of Chemistry, Faculty of Science, Universiti Teknologi Malaysia, 81310 UTM Johor Bahru, Johor, Malaysia

Received 21 October 2015; accepted 27 March 2016
Available online 11 April 2016

KEYWORDS

1,2-Dichlorobenzene;
TiO_2 rutile;
Surface defects;
Immobilization;
Thin film;
Response surface methodology

Abstract Photodegradation of 1,2-dichlorobenzene over illuminated trimetallic oxide consisting of rutile TiO_2 in major portion together with WO_3 and SnO_2 was studied with respect to the effect of physicochemical properties of the catalyst. The photocatalytic activity enhancement by the presence of surface defects due to calcination temperature was investigated with the information obtained from XRD, DRUV, PL, FESEM and XPS. Calcination of TiO_2 at 950 °C resulted in highest activity. Decrease in percentage of degradation of 1,2-dichlorobenzene was noted when it was immobilized on PVC film and chitosan beads. The effect of calcination temperature, catalyst loading and pH was investigated for slurry and after immobilization. Further optimization study was carried out with the aid of response surface methodology utilizing Box–Behnken design. High correlation was obtained for the experimental and the predicted value (R^2 = 0.9992, Adj. R^2 = 0.9982 and Pred. R^2 = 0.9971). Optimization result showed that the maximum percentage of degradation was achieved at calcination temperature of 961.2 °C, with catalyst loading of 0.22 g and pH 7.2. The presence of two intermediates was identified during the reaction using GC–MS. On top of that the photocatalyst could also be reused for several times.

1. Introduction

Chlorinated organic compounds have attracted wide attention due to their toxicity and bioaccumulation. It has been a challenging task to decompose the chlorinated volatile organic compounds such as 1,2-dichlorobenzene (DCB). Most of the research works conducted on DCB was in gas phase using catalytic oxidation method and only few photocatalytic studies were employed in aqueous medium. In aqueous systems, chlorinated hydrocarbons exhibit low chemical

* Corresponding author.
E-mail address: wazelee@kimia.fs.utm.my (W.A. Wan Abu Bakar).
Peer review under responsibility of King Saud University.

Production and hosting by Elsevier

http://dx.doi.org/10.1016/j.arabjc.2016.03.006

reactivity and non-biodegradability due to its toxicity (Mahmoud et al., 2012). In earlier study by Lin et al. (2002), TiO_2 with fluorinated surface has been used for the photodegradation of 1,2-dichlorobenzene in aqueous under UV light. Comparison of 1,4-dichlorobenzene photodegradation under UV and visible light was conducted by Mahmoud et al. (2012) which showed a slower degradation rate under visible light.

Alternatively, binary metal oxides have been explored and displayed better catalytic activity compared to pure TiO_2. Study by Tae Kwon et al. (2000) showed that WO_3 doped TiO_2 demonstrated higher photocatalytic activity under UV light compared to TiO_2 doped with SiO_2, SnO_2, Al_2O_3 and ZrO_2. Song et al. (1999) claimed that Ag/TiO_2 P25 presented higher catalytic activity compared to Cu/TiO_2 catalyst. TiO_2 P25 doped with SB, Nb and Bi metal ion by sol–gel method had been studied by Whang et al. (2005), with TiO_2/Nb found to show good catalytic activity. On another study by the same group, Nd^{3+} doped TiO_2 P25 was reported to exhibit higher catalytic activity compared to silica doped TiO_2 (Kim et al., 2006a, 2006b). Chetty et al. (2012) reported remarkable photocatalytic activity and stability was achieved by using Ni/TiO_2 for DCB degradation in the presence of ozone. Photodegradation of 1,4-dichlorobenzene under visible light was conducted by Chakraborty and Kebede (2011) using In_2O_3/TiO_2 composite with In_2O_3 acting as sensitizer for TiO_2 by absorbing visible light. All of these studies had reported the same fundamental process that took place in the enhancement of the photocatalytic activity which is the photogenerated charge transfer between the conduction band and valence band of the metal oxides. However, these oxides might be susceptible to catalytic deactivation due to adsorption of dissociative chloride ion that is generated from the decomposition processes. It has been reported that the incorporation of SnO_2 could avoid the poisoning of the catalyst and enhance the catalytic activity (Li et al., 2014; Mao et al., 2015).

In early years, enhanced photocatalytic degradation of organic compounds has been associated with the use of anatase TiO_2 or TiO_2 P25 mixture of anatase/rutile catalyst in nanoparticle size with low surface area. On contrary, recent studies have demonstrated that single catalyst as rutile TiO_2 (X. Liu et al., 2014), ZnO (X. Zhang et al., 2014), WO_3 (Xie et al., 2012), SnO_2 (Wang et al., 2015) and CeO_2 (Jiang et al., 2015) with high crystallinity, large particle size with exposed facets and low surface area showed higher photocatalytic activity under visible light. Another important characteristic that has been described to influence the photocatalyst performance was the presence of surface defects. Yan et al. (2013) have mentioned that the existence of surface/bulk defects on anatase and rutile TiO_2 improved the separation of photogenerated electron–hole pairs on TiO_2 upon irradiation and thus increased the photocatalytic reaction. Recently, hydrogenated TiO_2 (Amano and Nakata, 2014; Jiang et al., 2012; Zheng et al., 2012; Zhou et al., 2014) and reduced TiO_2 (W. Fang et al., 2014; W.Q.I. Fang et al., 2014; Mao et al., 2014; Ren et al., 2015) have triggered extensive research interest because of the band gap narrowing and reduction of electron–hole recombination due to the synergistic presence of oxygen vacancies and surface disorder on TiO_2.

Besides the surface modification of the catalyst, as mentioned above charge transfer and charge separation are the most essential aspects in photocatalytic reaction. Developing TiO_2 based multi-heterogeneous photocatalyst by surface modification has been an effective strategy for charge carrier transfer in enhancing the separation of photogenerated electron and holes. The efficiency of charge transfer and separation depends on the position of conduction band and valence band of the metal oxides. A wide range of bimetallic oxides such as TiO_2/WO_3 (Luevano-Hipolito et al., 2014), TiO_2/SnO_2 (Sasikala et al., 2009), TiO_2/ZnO (Hernandez et al., 2014), TiO_2/CeO_2 (Deng et al., 2015) and trimetallic oxide heterostructures $ZnO/TiO_2/SnO_2$ (Yang et al., 2012), SnO_2/rutile TiO_2/anatase TiO_2/Pt (Zhao et al., 2014), SnO_2/TiO_2/CdS (Gao et al., 2015), TiO_2/WO_3/Pt (Wang et al., 2014) have been explored to demonstrate high photocatalytic activity under visible light due to the efficient charge separation and transfer. Meanwhile, the formation of heterojunction on binary metal oxides with exposed facets has also been reported to enhance the activity due to the improved charge carrier separation (Liu et al., 2015).

Based on the above discussion, developing highly active catalysts that are environmentally friendly, cheap and stable is of importance. Therefore, we planned to synthesize multiheterostructure by coupling TiO_2 with WO_3 and SnO_2. All the three metal oxides have different potential energies with conduction band of SnO_2 and WO_3 positioned to be lower than TiO_2 (Yu et al., 2013; Zhang et al., 2013). This would form a staggered band structure that could promote the charge transfer and separation for photocatalytic reaction improvement. Besides, it is known that addition of WO_3 increases the surface acidity of the catalyst, thereby promoting the adsorption of water molecule and enhancing the formation of hydroxyl ion which is important in photodegradation reaction (Grabowska et al., 2012). Moreover WO_3 acts as an electron acceptor whereby W^{6+} can easily be reduced to W^{5+} which further improves the photogenerated charge carriers separation (Riboni et al., 2013) while incorporation of SnO_2 could avoid the deactivation of the catalyst. In addition, the mixed oxide TiO_2/WO_3 and TiO_2/SnO_2 with surface defects has been reported to enhance the photocatalytic activity under visible light irradiation (S. Liu et al., 2014; Yu et al., 2013). Thus in the preparation of multiheterostructure $TiO_2/SnO_2/WO_3$, surface defects on the metal oxides have been adjusted by calcination at optimum temperature (result not shown) while mechanical mixing was employed to minimize the structural deterioration. The effect of surface defects and the efficiency of charge transfer in the trimetallic oxides towards the photodegradation of DCB has been explored in this study. In addition to this, the effect of solution pH and photocatalyst loading was considered as well. As most studies on photodegradation were done in slurry mode which is not applicable for industrial use, in this research the performance of photocatalyst immobilized on support materials has been explored. The optimum condition using photocatalyst immobilized on support material was determined using response surface methodology (Box–Behnken design). Response surface methodology (RSM) has been proven to be a useful technique to evaluate the optimum condition and the relative significance of several affecting factors (Jiang et al., 2013). To our knowledge, the use of $TiO_2/SnO_2/WO_3$ photocatalyst immobilized on support material for the photodegradation of 1,2-dichlorobenzene under visible light and the optimization study has not been reported yet.

2. Material and methods

2.1. Materials

Titanium tetraisopropoxide (TTIP), tungstic acid (H_2WO_4) and chitosan with low molecular weight were purchased from Sigma Aldrich, tin (IV) chloride ($SnCl_4{\cdot}5H_2O$) from QreC while diethanolamine (DEA), polyethylene glycol (PEG 2000), polyvinyl chloride (PVC), tetrahydrofuran (THF) and acetonitrile were from Merck. Ethanol (EtOH) and hydrogen peroxide 30% solution were obtained from Qrec. 1,2-Dichlorobenzene (DCB) was purchased from BDH (purity > 99%). The stock solution of these compounds was prepared separately at a concentration of 1000 ppm in acetonitrile/water (35:65). The standard solution containing 100 ppm of DCB was prepared by diluting the stock solution with distilled water.

2.2. Preparation of sol–gel/Hydrothermal photocatalyst

The powder photocatalyst of TiO_2, WO_3 and SnO_2 was prepared according to the following modified procedure. TiO_2 was prepared by the hydrolysis and condensation reaction of

TTIP with EtOH. The TiO_2 sol solution was prepared by mixing PEG 2000:EtOH:DEA:TTIP:H_2O in the ratio of 1.1:43.7:3.8:7.5:1 one after another (Ali and Hassan, 2008). WO_3 sol solution was prepared by dissolving 5.4 g of tungstic acid in 100 mL of hydrogen peroxide solution and stirred to colourless, followed by the addition of PEG (1.35 g) after it was aged for one day (Tada et al., 2004). To prepare SnO_2 sol solution, 8.76 g of $SnCl_4{\cdot}5H_2O$ was dissolved in 100 mL of ethanol/water mixture in 1:1 ratio (Liu et al., 2006). The sol solutions were then transferred to Teflon vessels and heat treated at 170 °C for 5 h. The obtained product of WO_3 and SnO_2 was filtered and dried in oven at 95 °C. The filtered TiO_2 was left at room temperature to form xerogel and then it was dried in oven. In order to determine the effect of surface defects at different calcination temperatures, TiO_2 as the major component was chosen. The dried TiO_2 was calcined at 850 °C, 950 °C and 1050 °C for 5 h to study the thermal effect while WO_3 and SnO_2 were calcined at 850 °C for 5 h. All the calcined products were ground to fine powders.

Trimetallic oxide $TiO_2/SnO_2/WO_3$ in the optimum atomic ratio of 80:10:10 (from unpublished report), was mixed for 15 min using shaker at a speed of 150 rpm and followed by mechanical grinding. Three sets of trimetallic oxide were prepared and labelled as T(x)/SnO_2/WO_3 with x referred to TiO_2 calcination temperature (x = 850 °C, 950 °C and 1050 °C).

2.3. Preparation of immobilized photocatalyst

The prepared photocatalyst powder was immobilized on two different polymers: (i) PVC as synthetic polymer and (ii) chitosan as the natural polymer. The PVC was prepared in thin film form while chitosan was prepared in beads form.

For the preparation of PVC thin film, 1 g of polyvinyl chloride powder was slowly dissolved in 25 mL of THF solution under vigorous stirring. The obtained clear solution was then poured onto a Petri dish and left for 10 min till the solution starts to solidify. The prepared photocatalyst was spread on top of the semi-solid PVC layer and left overnight to dry. It has to be noted that the formation of semi-solid PVC layer is very important as overdrying would lead to leaching of the catalyst as the catalyst would not be completely held on the film. The dried thin film was then dried at 95 °C for 1 h to remove any moisture.

To prepare the photocatalyst immobilized in chitosan, 1 g of low molecular weight commercial chitosan powder was first dissolved in 2% acetic acid solution and then followed by the addition of 1 g photocatalyst sample. The mixture solution was kept stirring overnight. Then this mixture was added dropwise into 0.5 M NaOH solution to form the beads. The chitosan beads embedded with photocatalyst were filtered and washed several times with distilled water to remove any excess NaOH. The beads were dried in oven at 60 °C.

2.4. Photocatalytic activity measurement

Photocatalytic degradation of DCB was carried out in a pyrex reactor placed in a dark box with the inner part covered with aluminium foil. A compact fluorescence visible lamp (λ > 400 nm, Philips, 36 W) was placed next to the reactor. The experiments were performed with 250 mL solution containing 100 ppm DCB added with 0.1 g of photocatalyst either in powder form or with immobilized photocatalyst. Before illumination, the dispersion was magnetically stirred for 30 min in the dark to allow for adsorption of DCB onto the surface of the photocatalyst. Aliquots of the solution were collected at different time intervals for a total of 240 min. The aliquots were filtered using 0.45 μm membrane filter and directed to UV–Vis spectrophotometer to check the degradation of DCB via its absorption peak at 269 nm. This absorption data was used in the determination of degradation of DCB through comparison with the absorbance at a certain time as a percentage of the initial absorbance.

In order to study the effect of pH, the pH of the solution was adjusted from 4 to 10 by using 0.1 M NaOH or HCl. Meanwhile to study the the effect of catalyst loading, the amount of the catalyst was varied from 0.05 g to 0.40 g. Both the studies were conducted using catalyst in powder form and after immobilization.

2.5. Material characterization

The powder diffraction patterns were recorded by X-ray diffractometer Bruker AXS D5000 utilizing Cu Kα radiation with wavelength 0.15406 nm at 40 kV and 30 mA. Data were collected over the range of 20–80° at 0.050° intervals with 1 s count accumulation per step. The BET specific surface areas of the samples were measured by N_2 adsorption/desorption isotherms on a Micrometrics ASAP 2020 analyser. Surface morphologies were investigated using field emission scanning electron microscopy (FESEM, SU8020, Hitachi). Transmission electron microscopy (TEM) and high-resolution transmission electron microscopy (HRTEM) were performed on a JEOL JEM-2010 electron microscope. The diffuse reflectance UV–Vis (DRUV) spectra were taken using a Perkin Elmer Lambda 35 spectrophotometer. The surface electronic states of the samples were determined by X-ray photoelectron spectroscopy (XPS) on Axis Ultra DLD, Shimadzu/Kratos. All the binding energies were calibrated using the contaminant carbon (C 1s = 284.5 eV) as the reference. Atomic Force Microscopy (AFM) and Seiko model SP13800N with contact tip cantilever were used to record the surface roughness. The sample size of 1 μm × 1 μm was placed on Dynamic Force Mode (DFM) sample holder for measurement and software NanoNavi Analysis was used to analyse the data.

For the determination of the by-products, gas chromatograph Perkin Elmer (Clarus 680) with a 30 m, 0.25 mm HP-5MS capillary column coupled with Perkin–Elmer SQ8 mass detector operating at EI mode at 70 eV was utilized. During the reaction 5 mL sample was collected before and after every hour of photodegradation. The solution was extracted using 3 × 3 mL of isooctane and then added with anhydrous sodium sulphate. The collected organic solution was evaporated and then analysed using gas chromatography–mass spectrometry (GC–MS).

2.6. Experimental design

In this study, the optimization of experimental condition for the degradation of 1,2-dichlorobenzene was conducted with the aid of response surface methodology using Box–Behnken design. The study was conducted using Design expert software

version 7. Three independent parameters, (i) calcination temperature, (ii) pH and (iii) catalyst loading were varied for the optimization of photodegradation of 1,2-dichlorobenzene. The experimental design was constructed using two coded value for each variable, maximum (+1) and minimum (−1) which are equally spaced as shown in Table 1. The model is expressed by a second order polynomial function defined by Eq. (1):

$$Y(\%) = \beta_0 + \sum \beta_i X_i + \sum \beta_{ii} X_i^2 + \sum \beta_{ij} X_i X_j \quad (1)$$

where Y is the optimum predicted response, hereby is the percentage of DCB degradation. β_0 is the regression intercept, β_i is the regression for linear while β_{ii} and β_{ij} are the regression coefficients of square and interaction between the effects respectively. A total of 17 experiments were performed in randomized order as required by the design. The adequacy of the proposed model is then revealed using the diagnostic test provided by analysis of variance (ANOVA). Regression analysis is used to get the fitted quadratic polynomial equation, and then use the equation to develop the response surfaces and contour plots.

3. Results and discussion

3.1. Characterization of the catalyst

The X-ray diffraction (XRD) patterns for $TiO_2/SnO_2/WO_3$ with TiO_2 calcined at different temperatures are depicted in Fig. 1. The TiO_2 calcined at 850–1050 °C exists in pure rutile phase with peaks at 2θ = 27.4°, 36.0° and 41.2° denoted to hkl of (110), (101) and (111) which is consistent with reference data JCPDS no. 089-4202. SnO_2 nanoparticles with cassiterite type tetragonal form, presented peaks at 2θ = 26.5° (110), 33.8° (101) and 39.0° (111) that matched well with JCPDS no. 072-1147. Meanwhile WO_3 exists in monoclinic form (JCPDS no. 072-0677) with the main peaks at 2θ = 23.1°, 23.5°, 24.3° that indicates the presence of hkl plane (002), (020) and (200) respectively. The increase in calcination temperature of TiO_2 causes peak narrowing and increased in intensity which signifies grain growth and improved in crystallinity. It has been reported that rutile TiO_2 (X. Liu et al., 2014) and rutile SnO_2 (Wang et al., 2015) have active facet at crystal plane (110) and (111) while for monoclinic WO_3 it follows the order of (002) > (020) > (200) (Xie et al., 2012). From the XRD pattern, it could be noted that $T1050/SnO_2/WO_3$ has the highest (110) and (111) TiO_2 peak with low intensity of WO_3 (020) peak while $T850/SnO_2/WO_3$ has lower TiO_2 peak intensity with increased intensity of WO_3 (200) peak. Among all the three samples, $T950/SnO_2/WO_3$ showed balanced peak intensity which

Table 1 Experimental range and level of independent variables for photodegradation of DCB.

Independent variable	Range and levels		
	−1	0	+1
Calcination temperature of TiO_2, X_1 (°C)	850	950	1050
pH, X_2	5	7	9
Catalyst loading, X_3 (g)	0.10	0.25	0.40

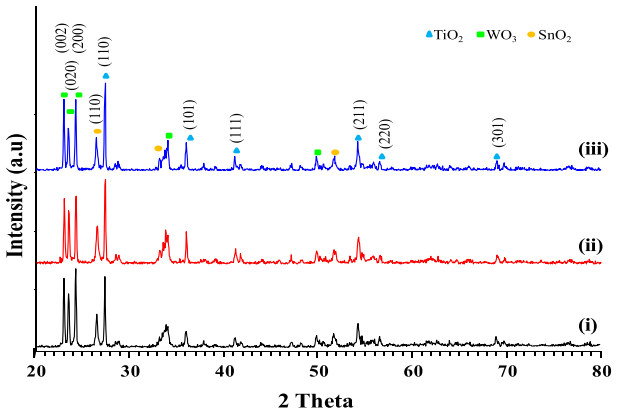

Figure 1 The X-ray diffraction (XRD) patterns for (i) $T850/SnO_2/WO_3$, (ii) $T950/SnO_2/WO_3$ and (iii) $T1050/SnO_2/WO_3$ phtocatalyst.

indicate the presence of active facets in proper ratio. No other significant changes were observed indicating no substitution of Sn or W into the lattice of TiO_2 in this physical mixing. Similar observation was reported by Wu et al. (2013) in the $MnO–CeO_2$ catalyst prepared by grinding using a mortar.

The high calcination temperature may have an impact on the lattice strain and thus Williamson–Hall equation (Eq. 2) was used to obtain the particle size of TiO_2 (Mote et al., 2012).

$$(\beta \cos\theta)/\lambda = 1/D + (\varepsilon \sin\theta)/\lambda \quad (2)$$

where 2θ is Bragg angle, λ is wavelength of X-ray used (Cu Kα in this case), β is full width at half maxima (FWHM), D is crystallite size, and β is effective strain in the lattice. Fig. 2 illustrates the Williamson–Hall plot the samples. The slope of straight line of (β cos θ/λ) vs. (sin θ/λ) represents the effective strain which originate from structural imperfections such as defects while the reciprocal of the intercept gives the crystallite size. The calculated particle sizes for $T850/SnO_2/WO_3$, $T950/SnO_2/WO_3$ and $T1050/SnO_2/WO_3$ are 73 nm, 99 nm and 462 nm respectively.

The effect of TiO_2 calcined at different temperatures on the optical and electronic properties of the trimetallic oxides was evaluated. The absorption of light obtained from diffuse reflectance UV is displayed in Fig. 3a. The absorption edge for all the samples falls in the visible region (λ > 400 nm) which indicates that the entire sample is active at visible light, with

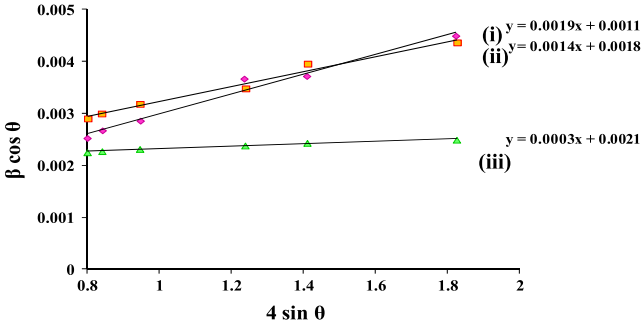

Figure 2 Particle size determination from Williamson–Hall plot derived from X-ray diffraction (XRD) data of (i) $T850/SnO_2/WO_3$, (ii) $T950/SnO_2/WO_3$ and (iii) $T1050/SnO_2/WO_3$.

enhanced absorption property observed for T950/SnO_2/WO_3 photocatalyst. The enhancement of the light absorption intensity may be attributed to the presence of oxygen vacancies and Ti^{3+} (Sekiya et al., 2000) which could be further verified from XPS data. The band gaps of the samples were determined from the $[F(R)hv]^{1/2}$ versus photon energy (hv) plot as shown in Fig. 3b (Zhang et al., 2015). It could be noted that each spectrum has two slopes. Therefore extrapolating the linear region of the curve gives the band gap values for T850/SnO_2/WO_3, T950/SnO_2/WO_3 and T1050/SnO_2/WO_3 as 2.59/2.77 eV, 2.46/2.55 eV and 2.57/2.74 eV respectively. As there is no doping between the metal oxides, the existence of two band gaps in these samples could be related to the vast difference in the conduction band energy of the metal oxides (Zhang et al., 2015).

Further verification on the nature of surface defects and chemical state of the metal oxides was carried out using XPS that is known for its surface sensitive analysis. The deconvolution of Ti, Sn, W and O is displayed in Fig. 4. The curve fitting done for Ti leads to three different environments. The binding energy of Ti $2p_{3/2}$ and $2p_{1/2}$ centred at 458.35–458.60 eV represents Ti^{4+} in bulk while peak at higher binding energy (459.46–459.80 eV) is suggested to be due to structural defects (Baia et al., 2014). The third peak at lower binding energy which is referred to the presence of Ti^{3+} was detected in sample T950/SnO_2/WO_3 and T1050/SnO_2/WO_3 only which is due to the effect of calcination temperature on TiO_2. The larger amount of Ti^{3+} was observed in T950/SnO_2/WO_3 (9.96%) but reduced to 4.41% in T1050/SnO_2/WO_3 due to increased crystallinity. For Sn (Fig. 4b), two doublets were observed with their spin orbit of $3d_{5/3}$ and $3d_{3/2}$. Several research works have referred the presence of two doublets with the existence of Sn^{2+} and Sn^{4+}. However the binding energy for Sn^{2+} according to the NIST database is 485.6 eV. Thus in this study, the first peak centred at 486.20–486.37 eV ($3d_{5/2}$) with the major portion, was attributed to Sn^{4+} in bulk while a smaller ratio at higher binding energy (486.99–487.05 eV) is suggested to be due to the structural defect as observed in the Ti. Meanwhile, the curve of W 4f spectra was fitted with three pairs of spin orbit ($4f_{7/2}$ and $4f_{5/2}$). The reduced W^{5+} was observed at low binding energy (34.03–34.13 eV) in all the samples with different ratios. The second $4f_{7/2}$ peak at binding energy 35.03–35.29 eV was denoted as W^{6+} while the third peak at higher binding energy (35.81–36.60 eV) was referred to structural defect. The presence of surface structural defects at the higher binding energy in each metal (as shown in Fig.4a–c) could be attributed to the surface atomic disorder caused by changes in the bonding and lattice strain upon calcination at high temperature (Sun, 2003). The amounts of W^{5+} present in T850/SnO_2/WO_3, T950/SnO_2/WO_3 and T1050/SnO_2/WO_3 are 4.2%, 14.4% and 9.4% respectively. Compared to the single WO_3 with only 3.6% W^{5+} (result not shown), the larger amount of W^{5+} in all the trimetallic oxides signifies the occurrence of charge transfer towards WO_3. This is in agreement with observation by Wu et al. (2013). Furthermore, the observed shift in the binding energies of Sn and W also indicates the interaction between the metal oxides (G. Zhang et al., 2014).

The formation of Ti^{3+} and W^{5+} also indicates the existence of oxygen vacancies which could be determined from the amount of adsorbed oxygen species. The asymmetric XPS spectrum of O 1s peak (Fig. 4d) revealed the presence of different oxygen species on the surface of the photocatalyst. The peak at binding energy around 530.0 eV, 531.5 eV and 532.9 eV could be ascribed to the lattice oxygen, oxygen vacancies or surface adsorbed oxygen and surface adsorbed H_2O (Li et al., 2014; X. Zhang et al., 2014). T950/SnO_2/WO_3 photocatalyst demonstrated the highest concentration of Ti^{3+}, W^{5+} and oxygen vacancies which is advantageous for the enhancement of photocatalytic activity.

Since the recombination of excited electrons and holes can amplify the PL emission signal, photoluminescence emission is a significant technique to investigate the separation efficiency of the photogenerated charge carriers in a semiconductor (Choudhury and Choudhury, 2014). Fig. 5 shows the photoluminescence spectra attained for all the photocatalysts which were almost identical in shape and position. The emission peaks that appeared between 420 nm and 465 nm may be attributed to the emission of band gap transition with the energy of emission corresponding to the band gap energy between different valence bands and conduction bands that exist in the trimetallic oxides. Meanwhile, the secondary PL emission peaks at 500 nm and above may be attributed to defects in the samples (Zhang et al., 2015). The emission intensity of T950/SnO_2/WO_3 that is lower than T850/SnO_2/WO_3 and T1050/SnO_2/WO_3 (Fig. 5) signifies a lower recombination rate of photogenerated electrons and holes. This could be correlated to the higher amount of oxygen vacancies that exist in T950/SnO_2/WO_3 resulting in a decreased PL intensity (Ma et al., 2014). Therefore, T950/SnO_2/WO_3 photocatalyst with suppressed electron–hole recombination rate is expected to increase the photocatalytic reaction.

Morphologies of the samples were characterized using FESEM and TEM. Fig. 6 clearly points out that all the samples are irregularly shaped. The surface morphology for

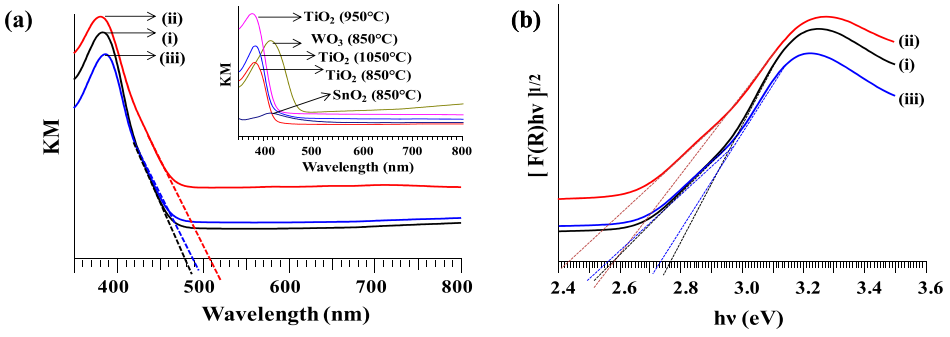

Figure 3 (a) Kubelka–Munk absorption curve for trimetallic oxide: (i) T850/SnO_2/WO_3, (ii) T950/SnO_2/WO_3 and (iii) T1050/SnO_2/WO_3 with inset plot for single metal oxides calcined at different temperatures. (b) Band gap of trimetallic oxides.

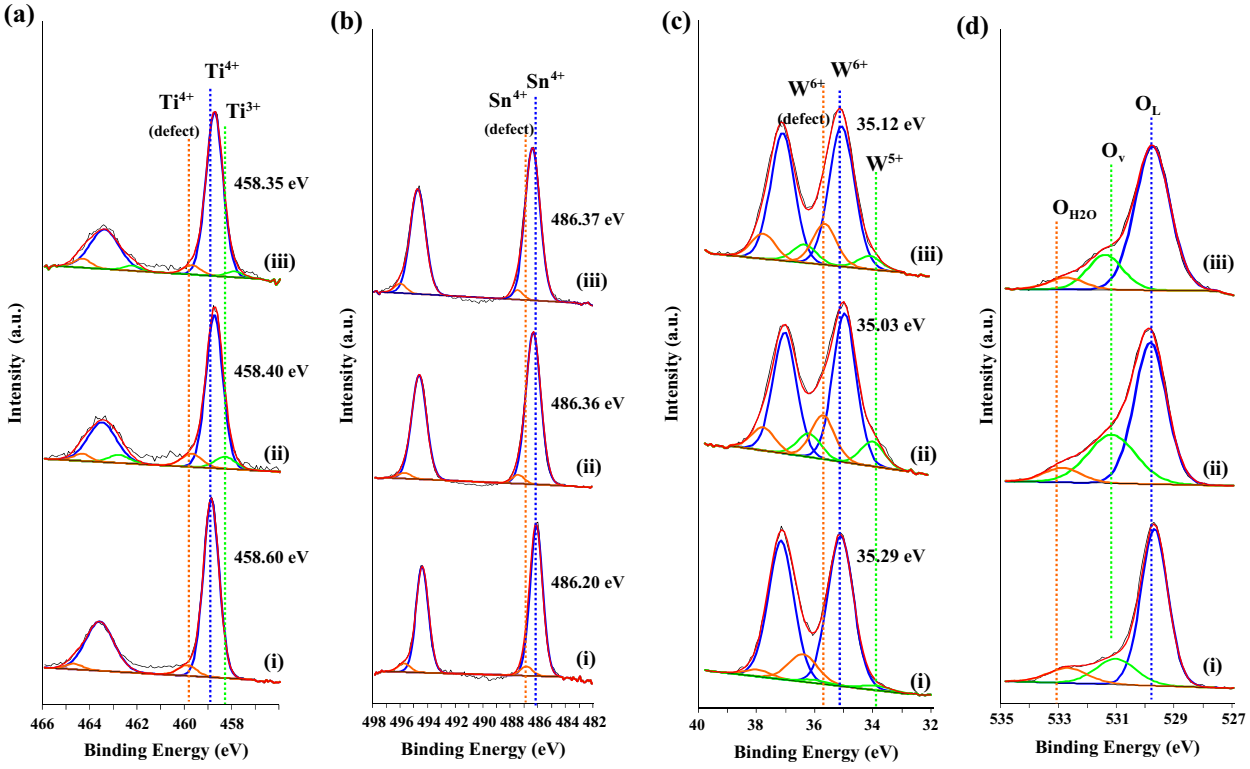

Figure 4 X-ray photoelectron spectroscopy of (i) T850/SnO_2/WO_3, (ii) T950/SnO_2/WO_3 and (iii) T1050/SnO_2/WO_3 photocatalyst showing the deconvolution for (a) Ti 2p, (b) Sn 3d, (c) W 4f and (d) O 1s.

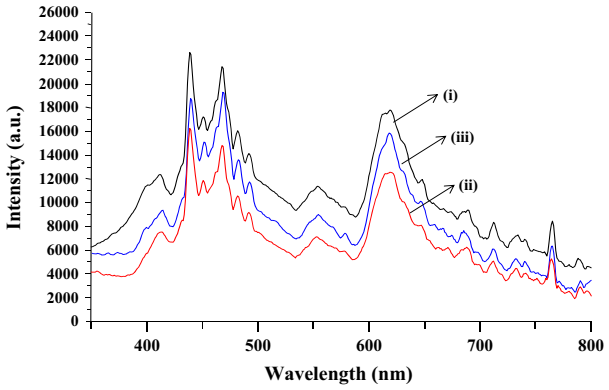

Figure 5 Photoluminescence spectra of (i) T850/SnO_2/WO_3, (ii) T950/SnO_2/WO_3 and (iii) T1050/SnO_2/WO_3.

T850/SnO_2/WO_3 photocatalyst obtained from FESEM (Fig. 6a), showed wide distribution of small agglomerated SnO_2 particles over TiO_2 calcined at 850 °C. With the increase in calcination temperature of TiO_2 to 950 °C, the existence of surface structural defects could be observed in T950/SnO_2/WO_3 that has sharp edges/cutting (Fig. 6b), but was not observed in T850/SnO_2/WO_3. These exposed surfaces with sharp edges are the reactive facets that contribute to their excellent activities in photocatalytic reaction. From Fig. 5b, it also revealed that the larger TiO_2 and WO_3 particles are closely bound with smaller SnO_2 particles partially adsorbed on the surface. However, further increase in the calcination temperature of TiO_2 to 1050 °C caused increase in the particle size as also revealed by XRD data. As shown by Fig. 6c, large particles could be seen in T1050/SnO_2/WO_3 catalyst. Even though the existence of facet could still be observed, the particles are not very closely bounded which might lead to inefficient charge transfer.

Meanwhile, Fig. 6d and e presents the surface morphology of the T950/SnO_2/WO_3 photocatalyst immobilized on PVC and chitosan. From Fig. 6d, it could be noted that the surface of the photocatalyst with sharp edges was slightly covered by the PVC while almost diminished when immobilized using chitosan (Fig. 6e). To further understand the contact between the metal oxides, image from TEM was obtained as shown in Fig. 6f. It could be seen from the TEM image that all the metal oxides are interconnected which is beneficial for the interparticle charge transfer and to improve the photocatalytic reaction. The HRTEM image has been presented in Fig. S2 (supporting document). Since the particle size calculated from XRD was large, the BET surface area obtained was low as shown in Table 2. The low surface area with small variation in BET surface area would not result in any obvious differences in the catalytic performance of the trimetallic oxide.

3.2. Effect of support on photocatalytic activity

The use of photocatalyst in powder form to study the reusability of catalyst is time consuming and might cause weight loss during the process of filtering and drying. This leads to the use of support materials. Hence, in this study PVC and chitosan were utilized as support materials. Based on the characterization, the potential photocatalyst T950/SnO_2/WO_3 was used to investigate the effect of support on photocatalytic

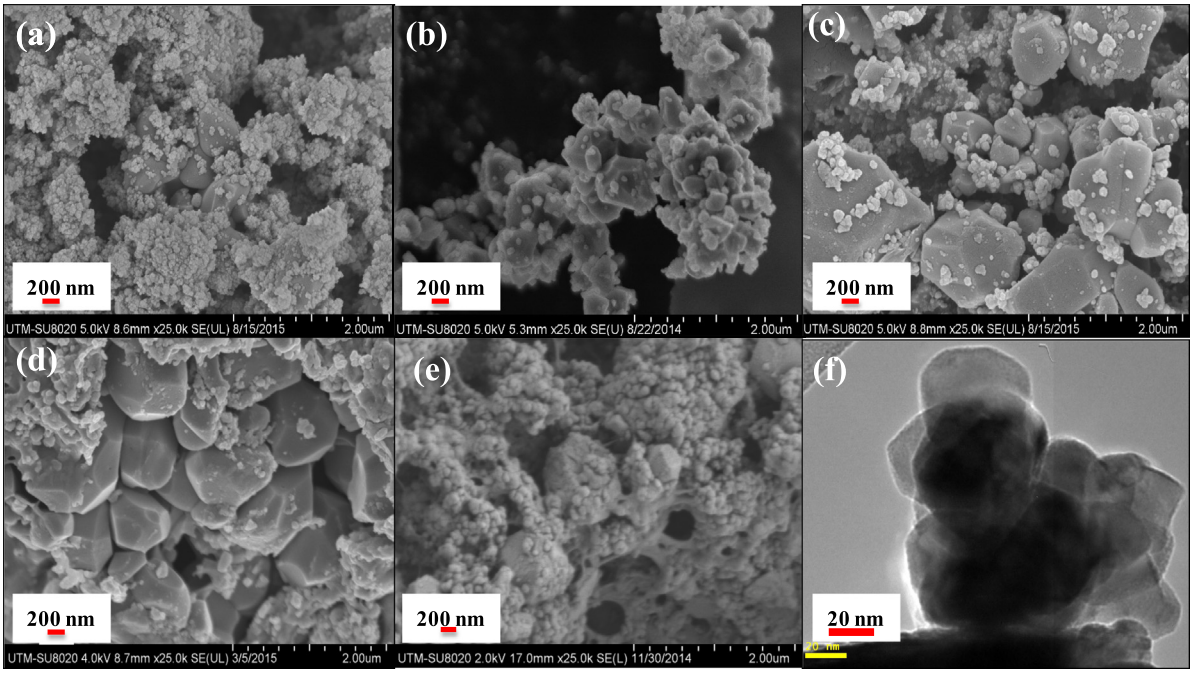

Figure 6 FESEM image of sample (a) T850/SnO_2/WO_3, (b) T950/SnO_2/WO_3, (c) T1050/SnO_2/WO_3, (d) T950/SnO_2/WO_3 immobilized on PVC film, (e) T950/SnO_2/WO_3 immobilized on chitosan beads and (f) TEM for T950/SnO_2/WO_3.

Table 2 BET specific surface area, total pore volume and average pore diameter for all the trimetallic oxide photocatalysts.

Sample	BET specific surface area (m^2/g)	Total pore volume (cm^3/g)	Average pore diameter (nm)
T850/SnO_2/WO_3	4.075	0.0395	106.73
T950/SnO_2/WO_3	2.720	0.0460	282.46
T1050/SnO_2/WO_3	1.599	0.0371	92.80

activity. To determine the efficiency of these support materials, photocatalyst immobilized on PVC and chitosan was compared with the powder photocatalyst. The experimental results (Fig. 7) showed that the activity decreased when the photocatalyst was immobilized on PVC and chitosan. Lower photocatalytic activity was observed when the photocatalyst was immobilized on chitosan. These results could be correlated with the method of preparation followed by surface morphologies obtained from FESEM.

Notably, the high activity was achieved when using powder photocatalyst which is due to the exposed surface that has large contact with the pollutants (Fig. 6b). However when the photocatalyst was spread on top of PVC film, the catalysts are now partially embedded in the film and not 100% of the surfaces are exposed (Fig. 6d). Thus, lesser amount of pollutants is in-contact with the exposed surface causing slight decline in the activity. On the other hand, during the immobilization with chitosan, the photocatalyst was mixed together with chitosan in acetic acid solution before forming chitosan beads. The chitosan polymer is highly porous material which is sufficiently packed to form beads (Guibal, 2005). In this case, the photocatalyst particles have been encapsulated within the chitosan polymer networks, therefore reducing large amount of catalyst with exposed surface (Fig. 6e). Hence, this observation could be directly related to the lower catalytic activity attained when photocatalyst in chitosan beads was

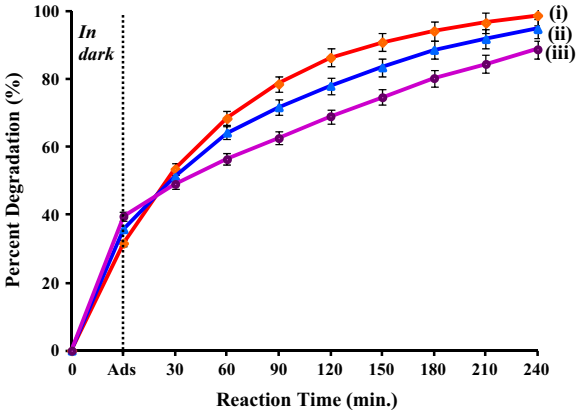

Figure 7 Photocatalytic degradation of 1,2-dichlorobenzene using T950/SnO_2/WO_3 photocatalyst (i) in powder form, (ii) immobilized on PVC film and (iii) immobilized on chitosan in beads form.

employed. Nevertheless, the higher dark adsorption observed could be associated with the adsorption capability of the porous structured chitosan (Sabar et al., 2015). Consequently, this study highlights the importance of photocatalyst with exposed surface for the photodegradation of DCB. Thus, the following

study on optimization was conducted using T950/SnO_2/WO_3 photocatalyst immobilized on PVC film.

3.3. Effect of calcination temperature

Calcination temperature plays an important role in surface morphology, structural defects and surface defects. Hence, in this study the effect of calcination temperature on one of the metal oxides was considered. As TiO_2 exists in major portion in this trimetallic oxide, the effect of calcination temperature was evaluated using TiO_2 calcined at different temperatures. Comparison with powder form photocatalyst was also conducted. The photocatalytic performances of the trimetallic oxide with different calcination temperatures are shown in Fig. 8. The photocatalyst in powder form demonstrated higher catalytic activity compared to when it was immobilized on PVC film. This could be correlated to the reduced number of exposed surface photocatalyst as discussed in Section 3.2. Both powder and immobilized photocatalyst exhibited the highest photodegradation of DCB when TiO_2 calcined at 950 °C was used in the trimetallic oxide. The UV absorbance spectrum for degradation of DCB using T950/SnO_2/WO_3 photocatalyst immobilized on PVC is displayed in Fig. S3 (supporting document).

The effect of calcination temperature on the photodegradation of DCB by using trimetallic oxide photocatalysts immobilized on PVC film over the reaction time is presented in Fig. 9. The photocatalytic activity of the single and binary metal oxides was included as well in Fig. 9 for comparison. It could be noted that all the metal oxides are active at visible light which is in agreement with UV–Vis absorption spectra (inset of Fig 3a). TiO_2 calcined at 950 °C showed high catalytic activity compared to WO_3 and SnO_2. In this study, SnO_2 showed fairly good catalytic activity under visible light which could be correlated to the existence of structural defect as depicted by XPS (Fig. 4b). The catalytic activity was improved when 10% of WO_3 was mixed with TiO_2. The enhancement of the photocatalytic activity was observed with the addition of 10% SnO_2 forming trimetallic oxide T950/SnO_2/WO_3 (80:10:10). On the contrary, T850/SnO_2/WO_3 demonstrated lower catalytic activity then the binary metal oxide which could be associated with

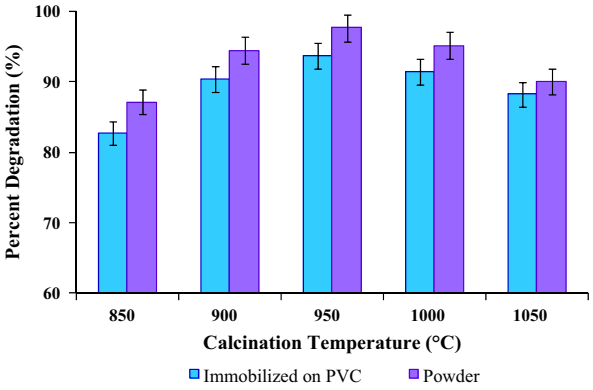

Figure 8 Photocatalytic degradation of 1,2-dichlorobenzene using Tx/SnO_2/WO_3 photocatalyst in powder form and immobilized on PVC film (with x referred to calcination temperature of TiO_2) conducted for 4 h under visible light.

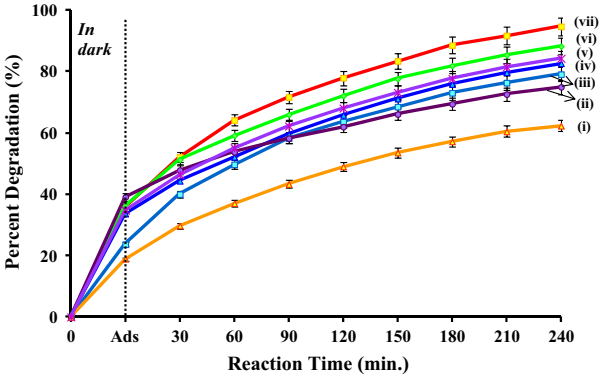

Figure 9 Photocatalytic degradation of 1,2-dichlorobenzene under visible light using (i) SnO_2, (ii) WO_3, (iii) TiO_2 calcined at 950 °C (T950), (iv) T850/SnO_2/WO_3, (v) T950/WO_3 (90:10), (vi) T1050/SnO_2/WO_3 and (vii) T950/SnO_2/WO_3 photocatalysts immobilized on PVC film.

the effect of TiO_2 calcined at 950 °C (T950). From Fig. 9, it could be noted that almost high adsorption of DCB was observed using the trimetallic oxides. The high adsorption of organic pollutant is essential for enhancing photocatalytic reaction. Nevertheless, even though TiO_2 with different calcination temperature was used in the trimetallic oxide photocatalyst, the variation in the per cent of adsorbed DCB was small. This could be related to the identical ratio of WO_3 in all the trimetallic oxides. As reported by Albonetti et al. (2008), in the presence of Lewis acid (TiO_2 and SnO_2) and Bronsted acid site (WO_3), DCB would initially be adsorbed on Bronsted acid site. This phenomenon is also true for pure WO_3 which has higher adsorption compared to TiO_2 and SnO_2. A comparison of the adsorption capability and photocatalytic reaction of DCB using T950/SnO_2/WO_3 for 4 h is displayed in Fig. S4 (supporting document).

The influence of surface defects on the behaviour of the trimetallic oxides is of particular interest that contributed to the distinction in the photocatalytic activity. Based on XPS data, the presence of Ti^{3+} in different concentrations was observed in T950/SnO_2/WO_3 and T1050/SnO_2/WO_3; however, Ti^{3+} was not observed in T850/SnO_2/WO_3. The deviation in the concentration of Ti^{3+} in TiO_2 was the effect of different calcination temperature. However, XPS analysis also revealed that all the trimetallic oxides have higher concentration of W^{5+} when compared to the pure WO_3 calcined at 850 °C. This data showed the occurrence of charge transfer between the metal oxides and formation of heterojunction by the interaction of metal oxides which is proposed in Scheme 1. In this reaction, the enhanced photocatalytic activity of the trimetallic oxide compared to the pure metal oxides could be due to two factors: (i) the improved charge transfer and charge separation by multiple pathways as proposed in Scheme 1 and (ii) the presence of high concentration of oxygen vacancies. As the conduction band of SnO_2 and WO_3 is lower than TiO_2, electrons in the conduction band of TiO_2 can be transferred to that of SnO_2 and WO_3 under visible light irradiation. Meanwhile holes from the lower valence band of SnO_2 and WO_3 could be transferred to TiO_2. This improves the separation and migration of photogenerated carriers and reduced the electron–hole recombination rate. A large number of electrons

on WO_3 generate more W^{5+} and increase the formation of $O_2^{\cdot-}$ while holes on TiO_2 surface increase the formation of OH^-. The formation of OH^- and $O_2^{\cdot-}$ is essential in the photodegradation of DCB in aqueous. Based on XPS analysis, the large concentration of W^{5+} was available on $T950/SnO_2/WO_3$ catalyst. In addition, it also has large amount of surface adsorbed oxygen. In the decomposition process, the released chloride ion would be adsorbed on the catalyst surface. The excess surface adsorbed oxygen improves the desorption of chloride ions and stabilizes the catalyst, thus enhanced the photocatalytic activity (Mao et al., 2015). The decrease in the photocatalytic activity therefore is related to the concentration of W^{5+} and oxygen vacancies.

3.4. Effect of pH

Photocatalytic reactions for DCB in solution with different pH levels are presented in Fig. 10. As it could be perceived, the photocatalytic activity increased with the increase in value of pH. It has been suggested that the effect of solution pH on the photocatalytic degradation is a complex subject associated with the reaction mechanism and the adsorption characteristics of substrate onto photocatalyst surface. According to the principle of heterogeneous photocatalysis, the concentration of OH^- ions is critical for the generation of $^{\cdot}OH$ radicals. Thus at higher pH value, the formation of hydroxyl ion was favoured (Huang et al., 2014). Nevertheless, it should be noted that the lifetime of $^{\cdot}OH$ radicals is very short and photocatalytic reactions can only take place at or near the surface of photocatalyst. Due to the non-ionic property of DCB, the neutral medium seems beneficial for the adsorption of DCB. As a result, considering the combined effect of the generation of OH^- and the interaction between DCB and the surface of the photocatalyst, the photocatalytic degradation of DCB was most efficient in neutral medium (Wang and Ku, 2007).

3.5. Effect of catalyst loading

Typically it is known that photocatalytic activity increases with catalyst loading up to a certain value beyond which the activity decreases. Similar experimental result was attained in this study which is presented in Fig. 11. The degradation efficiency rapidly increased with loading of photocatalyst of up to 0.25 g for powder sample and after immobilized on PVC film. Above this point, the photocatalytic activity started to decline. The influence of catalyst loading on the photodegradation of DCB can be explained in terms of the accessible exposed surface site for the adsorption of DCB and illuminated area which are essential to promote the photocatalytic reaction. The higher loading of powder photocatalyst caused excess of particles and increased the thickness of the photocatalyst in slurry mode. According to Choi et al. (2000), light penetration is exponentially extinguished along the depth while reaction rate is proportional to the absorbed light intensity. Therefore, the increase in thickness of catalyst particles leads to shielding effect or reduction of light penetration and decrease in activity. On the other hand, the higher loading of photocatalyst immobilized on PVC causes reduction of exposed surface photocatalyst. During the immobilization of photocatalyst on PVC, higher loading caused some of the catalyst to sink into PVC liquid due to the increase in density. The photocatalyst that sank in the PVC during preparation got embedded in the PVC film upon drying and therefore reducing the exposed surface of catalyst. To justify this statement, the surface roughness of immobilized photocatalyst with different loading was evaluated using AFM.

Fig. 12 portrays the three dimensional images of PVC film surface with photocatalyst loading of 0.25 g and 0.30 g. The differences in the surface roughness are shown by the images (Fig. 12) and by the root-mean-square roughness value (R_{rms}). The R_{rms} value for photocatalyst loading of 0.25 g is 7.293 nm and 4.630 nm for 0.30 g loading. The low R_{rms} value proves the reduction in the amount of catalyst exposed on surface (Stefanov et al., 2016). Consequently, the decrease in number of catalyst particles on PVC surface leads to reduction of adsorbed light intensity and the contact between photocatalyst and pollutant which caused the decline in activity.

3.6. Optimization of degradation conditions using RSM approach

For the response surface methodology involving Box–Behnken design, a total of 17 experiments were conducted for three factors at three levels (Table 1). The design used for the optimization and the responses observed and predicted for the 17 experiments are depicted in Table 3 (supporting document).

From the experimental design, an empirical second order polynomial equation was developed that correlates the response and the three different process variables as shown in Eq. (3):

$$Y = 95.70 - 1.19A - 0.93B + 0.34C + 0.20AB - 0.15AC + 0.11BC - 5.53A^2 - 2.58B^2 - 2.11C^2 \quad (3)$$

where Y represents per cent degradation (%) while A, B and C refer to the coded value of calcination temperature, catalyst loading and initial pH respectively. The predicted per cent degradation based on Eq. (3) has been tabulated in Table 3 for comparison with the experimental or observed value.

The experimental data for the degradation of DCB were statistically analysed by analysis of variance (ANOVA) and the result is displayed in Table 4 (supporting document). The significance of the model was determined by the variation attributed from the model and the experimental error; which is performed by F-value. Meanwhile, adequacy of the model is evaluated from the difference between the observed and the predicted response value (residual error). Hence, the ANOVA of the second order quadratic polynomial model for the response with model F-value of 1000.50 and its corresponding p-values of < 0.0001 showed that the model was significant. The property of the fit polynomial model was determined by the coefficient of determination (R^2) that quantitatively evaluates the correlation between the experimental data and the predicted response (Khataee et al., 2010). The R^2 value of 0.9992 is in good agreement with the adjusted R^2 (0.9982) and predicted R^2 (0.9971) which is considerably high, thus advocating a high correlation between the observed values and the predicted values. This indicates that the regression model provides an excellent explanation of the relationship between the independent variables and response. Furthermore the ANOVA result also showed that the lack of fit F-values of

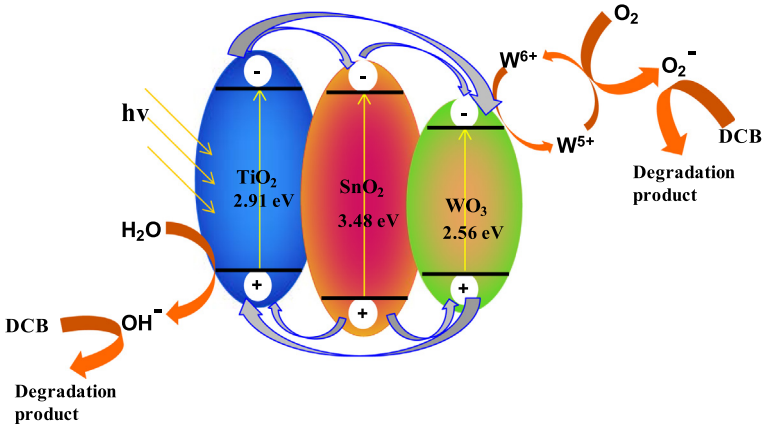

Scheme 1 Proposed schematic diagram for charge transfer in T950/SnO_2/WO_3 upon irradiation under visible light.

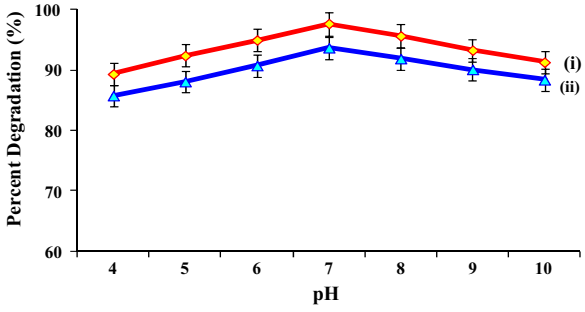

Figure 10 Photocatalytic degradation of 1,2-dichlorobenzene with 0.1 g T950/SnO_2/WO_3 photocatalyst (i) in powder form and (ii) immobilized on PVC film at different pH range, conducted for 4 h under visible light.

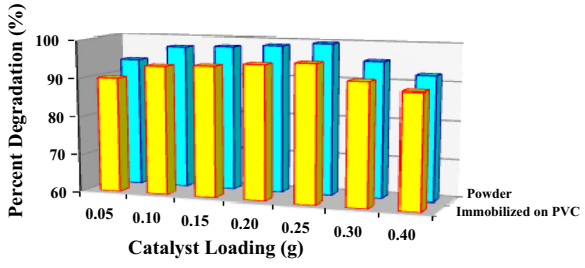

Figure 11 Photocatalytic degradation of 1,2-dichlorobenzene with T950/SnO_2/WO_3 photocatalyst in powder form and immobilized on PVC film at different catalyst loading. The reaction was conducted under visible light for 4 h.

0.24 implies that the lack of fit is not significant as the *p*-values were >0.05. The insignificant lack of fit confirmed the predictability of the model.

ANOVA results also indicate that all the independent variables of the quadratic polynomial model *A*, *B* and *C*, the interaction between calcination temperature with catalyst loading (*AB*) and the quadratic terms A^2, B^2 and C^2 are statistically significant as their *p*-values are <0.05. The most significant factor that influences the degradation of DCB as estimated by ANOVA is the effect of calcination temperature on the catalyst, followed by catalyst loading. The pH has a minor effect on the overall catalytic activity. The ANOVA result exemplified that the two-variable interactions had no significant effect on the pH ($p > 0.05$). The interaction between the variables and the optimum condition was further evaluated from the 3D plot of response surface shown in Fig. 13. From the surface response model, the optimized per cent degradation was estimated as 95.86% with calcination temperature of TiO_2 961.2 °C, catalyst loading of 0.22 g and pH 7.16. Verification of the estimated result at the proposed condition was carried out. The obtained experimental value of 95.84% is in good agreement with the predicted result of 95.89%, therefore validated the findings of response surface optimization. On the whole, ANOVA and the 3D plots illustrated that the calcination temperature plays the major role in structuring the catalyst surface and enhancing the photocatalytic activity at visible light.

3.7. Efficiency of the photocatalyst

For further affirmation of the efficiency of the photocatalyst, the decomposed by-product after 4 h of reaction was analysed by GC–MS (Fig. S5). After 4 h, the final by-product was identified as 4-chloro-4-hydroxy-3-butenal based on the mass spectra fragmentation ions (Scheme 2). Several other peaks obtained could not be identified from the MS spectra library. The removal of chloride ion was verified by the presence of AgCl white precipitate upon the addition of $AgNO_3$ and by the reduction of pH from 7.0 to 6.7.

It is also important to determine the stability and the reproducibility of the photocatalyst. Hence the photocatalyst was examined by repeating the reaction procedure. At the end of each reaction, the photocatalyst was cleansed using methanol and washed thoroughly using distilled water in order to get rid of any DCB compound or by-products adsorbed on the photocatalyst. The photocatalyst was then dried in oven at 80 °C for 30 min prior to reuse for the next reaction. Fig. 14 illustrates the performance of the T950/SnO_2/WO_3 photocatalyst after six consecutive runs with an average of 97% degradation which demonstrates the stability of the catalyst and thus its efficiency.

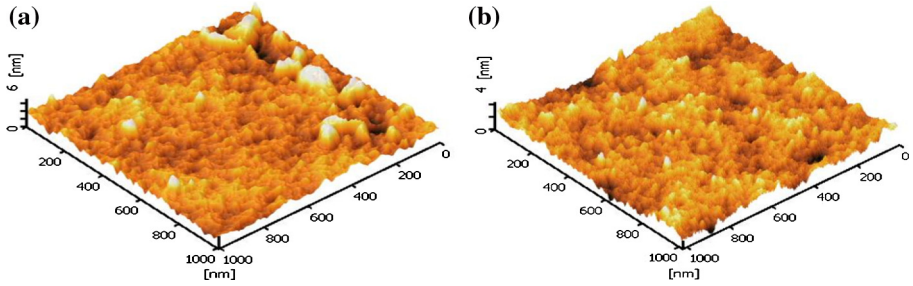

Figure 12 AFM image of T950/SnO_2/WO_3 immobilized on PVC with catalyst loading of (a) 0.25 g and (b) 0.30 g.

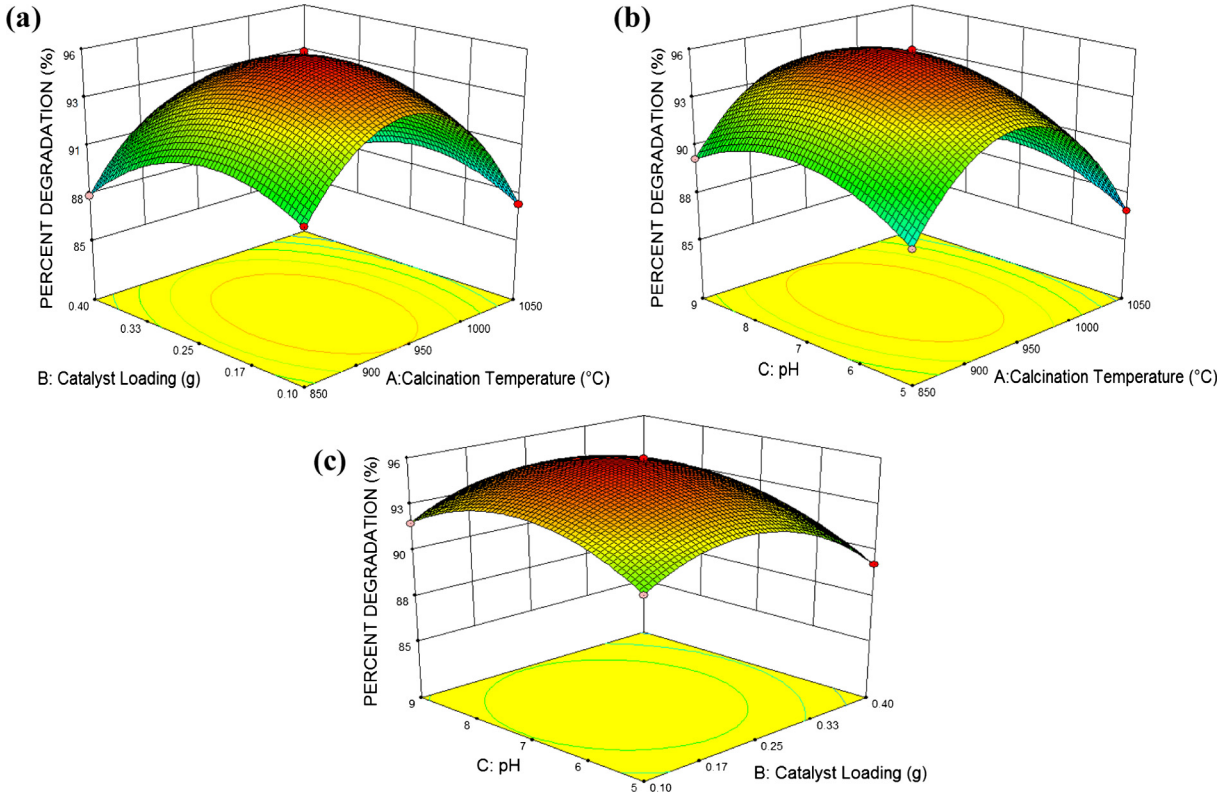

Figure 13 DCB per cent degradation and the interaction between (a) calcination temperature vs loading, (b) calcination temperature vs pH, and (c) catalyst loading vs pH presented in 3D surface response plot.

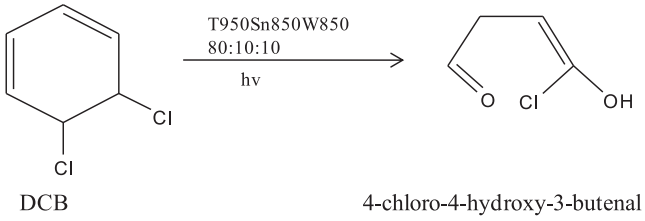

Scheme 2 By-product obtained from photodegradation of DCB using T950/SnO_2/WO_3 photocatalyst under visible light for 4 h.

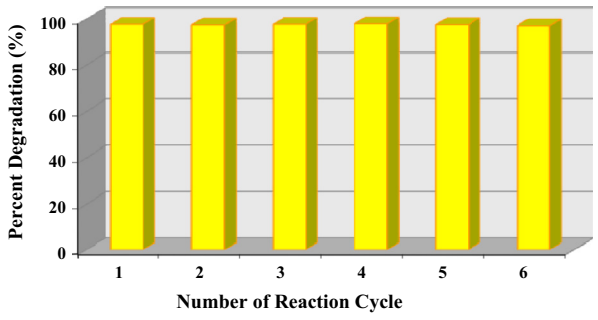

Figure 14 Reproducibility efficiency of T950/SnO_2/WO_3 catalyst immobilized on PVC film.

4. Conclusions

The performance of trimetallic metal oxide $TiO_2/SnO_2/WO_3$ in the ratio of 80:10:10 prepared from rutile TiO_2 calcined at 950 °C, WO_3 and SnO_2 calcined at 850 °C showed high degradation of DCB in aqueous under visible light. Comparison of the activity on different support materials showed that powder form > immobilized with PVC film > chitosan beads. An conventional way optimization study was conducted on the effect of calcination temperature, pH and catalyst loading which demonstrated that the optimum condition was obtained when TiO_2 calcined at 950 °C was used in the preparation of the trimetallic oxide with catalyst loading of 0.25 g and solution pH of 7. This result is in good agreement with optimization study using response surface methodology technique. ANOVA revealed that calcination temperature was the predominant factor influencing the photocatalytic activity which is related to the presence of surface defects. Therefore, in this study the enhanced photocatalytic activity was achieved due to the efficient charge transfer and the effect of large amount of oxygen vacancies. Meanwhile the detection of by-product during the reaction and the reproducibility of the photocatalyst $T950/SnO_2/WO_3$ verified the efficiency of the photocatalyst.

Acknowledgements

The authors are grateful to Universiti Teknologi Malaysia for financial support under GUP 04H97 and Ministry of Higher Education, Malaysia is acknowledged for the scholarship given to Renugambaal Nadarajan.

Appendix A. Supplementary material

Supplementary data associated with this article can be found, in the online version, at http://dx.doi.org/10.1016/j.arabjc.2016.03.006.

References

Albonetti, S., Blasioli, S., Bonelli, R., Mengou, J.E., Scirè, S., Trifirò, F., 2008. The role of acidity in the decomposition of 1,2-dichlorobenzene over TiO_2-based V_2O_5/WO_3 catalysts. Appl. Catal. A Gen. http://dx.doi.org/10.1016/j.apcata.2007.12.033.

Ali, R., Hassan, S.H., 2008. Degradation studies on paraquat and malathion using TiO_2/ZnO based photocalatyst. Malaysian J. Anal. Sci. 12, 77–87.

Amano, F., Nakata, M., 2014. High-temperature calcination and hydrogen reduction of rutile TiO_2: a method to improve the photocatalytic activity for water oxidation. Appl. Catal. B Environ. 158–159, 202–208. http://dx.doi.org/10.1016/j.apcatb.2014.04.025.

Baia, L., Vulpoi, A., Radu, T., Karacsonyi, E., Dombi, A., Hernadi, K., Danciu, V., Simon, S., Kovacs, G., Pap, Z., 2014. TiO_2/WO_3/Au nanoarchitectures' photocatalytic activity "from degradation intermediates to catalysts' structural peculiarities" Part II: aerogel based composites – fine details by spectroscopic means. Appl. Catal. B Environ. 148–149, 589–600. http://dx.doi.org/10.1016/j.apcatb.2013.12.034.

Chakraborty, A.K., Kebede, M.A., 2011. Efficient decomposition of organic pollutants over In_2O_3/TiO_2 nanocomposite photocatalyst under visible light irradiation. J. Clust. Sci. 23, 247–257. http://dx.doi.org/10.1007/s10876-011-0425-z.

Chetty, E.C., Dasireddy, V.B., Maddila, S., Jonnalagadda, S.B., 2012. Efficient conversion of 1,2-dichlorobenzene to mucochloric acid with ozonation catalyzed by V_2O_5 loaded metal oxides. Appl. Catal. B Environ. 117–118, 18–28. http://dx.doi.org/10.1016/j.apcatb.2012.01.004.

Choi, W., Hong, S.J., Chang, Y.S., Cho, Y., 2000. Photocatalytic degradation of polychlorinated dibenzo-p-dioxins on TiO_2 film under UV or solar light irradiation. Environ. Sci. Technol. 34, 4810–4815.

Choudhury, B., Choudhury, A., 2014. Oxygen defect dependent variation of band gap, Urbach energy and luminescence property of anatase, anatase-rutile mixed phase and of rutile phases of TiO_2 nanoparticles. Phys. E: Low-Dimens. Syst. Nanostruct. 56, 364–371. http://dx.doi.org/10.1016/j.physe.2013.10.014.

Deng, W., Dai, Q., Lao, Y., Shi, B., Wang, X., 2015. Low temperature catalytic combustion of 1,2-dichlorobenzene over CeO_2–TiO_2 mixed oxide catalysts. Appl. Catal. B Environ. 181, 848–861. http://dx.doi.org/10.1016/j.apcatb.2015.07.053.

Fang, W., Xing, M., Zhang, J., 2014. A new approach to prepare Ti^{3+} self-doped TiO_2 via $NaBH_4$ reduction and hydrochloric acid treatment. Appl. Catal. B Environ. 160–161, 240–246. http://dx.doi.org/10.1016/j.apcatb.2014.05.031.

Fang, W.Q.I., Huo, Z., Liu, P., Wang, X.L.U., Zhang, M., Jia, Y., Zhang, H., Zhao, H., Yang, H.G.U., Yao, X., 2014. Fluorine-doped porous single-crystal rutile TiO_2 nanorods for enhancing photoelectrochemical water splitting. Chemistry 20, 11439–11444. http://dx.doi.org/10.1002/chem.201402914.

Gao, C., Zhang, Z., Li, X., Chen, L., Wang, Y., He, Y., Teng, F., Zhou, J., Han, W., Xie, E., 2015. Synergistic effects in three-dimensional SnO_2/TiO_2/CdS multi-heterojunction structure for highly efficient photoelectrochemical hydrogen production. Sol. Energy Mater. Sol. Cells 141, 101–107. http://dx.doi.org/10.1016/j.solmat.2015.05.026.

Grabowska, E., Sobczak, J.W., Gazda, M., Zaleska, A., 2012. Surface properties and visible light activity of W-TiO_2 photocatalysts prepared by surface impregnation and sol–gel method. Appl. Catal. B Environ. 117–118, 351–359. http://dx.doi.org/10.1016/j.apcatb.2012.02.003.

Guibal, E., 2005. Heterogeneous catalysis on chitosan-based materials: a review. Prog. Polym. Sci. 30, 71–109. http://dx.doi.org/10.1016/j.progpolymsci.2004.12.001.

Hernandez, S., Cauda, V., Chiodoni, A., Dallorto, S., Sacco, A., Hidalgo, D., Celasco, E., Pirri, C.F., 2014. Optimization of 1D ZnO@TiO_2 core–shell nanostructures for enhanced photoelectrochemical water splitting under solar light illumination. ACS Appl. Mater. Interfaces 6, 12153–12167. http://dx.doi.org/10.1021/am501379m.

Huang, S.T., Lee, W.W., Chang, J.L., Huang, W.S., Chou, S.Y., Chen, C.C., 2014. Hydrothermal synthesis of $SrTiO_3$ nanocubes: characterization, photocatalytic activities, and degradation pathway. J. Taiwan Inst. Chem. Eng. 45, 1927–1936. http://dx.doi.org/10.1016/j.jtice.2014.02.003.

Jiang, D., Wang, W., Zhang, L., Zheng, Y., Wang, Z., 2015. Insights into the surface defect dependence of photoreactivity over CeO_2 nanocrystals with well-defined crystal facets. ACS Catal. 5, 4851–4858. http://dx.doi.org/10.1021/acscatal.5b01128.

Jiang, W., Joens, J.A., Dionysiou, D.D., O'Shea, K.E., 2013. Optimization of photocatalytic performance of TiO_2 coated glass microspheres using response surface methodology and the application for degradation of dimethyl phthalate. J. Photochem. Photobiol. A Chem. 262, 7–13. http://dx.doi.org/10.1016/j.jphotochem.2013.04.008.

Jiang, X., Zhang, Y., Jiang, J., Rong, Y., Wang, Y., Wu, Y., Pan, C., 2012. Characterization of oxygen vacancy associates within hydrogenated TiO_2: a positron annihilation study. J. Phys. Chem. C 116, 22619–22624. http://dx.doi.org/10.1021/jp307573c.

Khataee, A.R., Fathinia, M., Aber, S., Zarei, M., 2010. Optimization of photocatalytic treatment of dye solution on supported TiO_2 nanoparticles by central composite design: intermediates identification. J. Hazard. Mater. 181, 886–897. http://dx.doi.org/10.1016/j.jhazmat.2010.05.096.

Kim, E.Y., Kim, Y.H., Whang, C.M., 2006a. Nd^{3+}-doped TiO_2 nanoparticles prepared by sol-hydrothermal process. Mater. Sci. Forum 510–511, 122–125. http://dx.doi.org/10.4028/www.scientific.net/MSF.510-511.122.

Kim, E.Y., Whang, C.M., Lee, W.I., Kim, Y.H., 2006b. Photocatalytic property of SiO_2/TiO_2 nanoparticles prepared by sol-hydrothermal process. J. Electroceram. 17, 899–902. http://dx.doi.org/10.1007/s10832-006-9071-5.

Li, J., Zhao, P., Liu, S., 2014. SnOx–MnOx–TiO_2 catalysts with high resistance to chlorine poisoning for low-temperature chlorobenzene oxidation. Appl. Catal. A Gen. 482, 363–369. http://dx.doi.org/10.1016/j.apcata.2014.06.013.

Lin, H.F., Ravikrishna, R., Valsaraj, K., 2002. Reusable adsorbents for dilute solution separation. 6. Batch and continuous reactors for the adsorption and degradation of 1,2-dichlorobenzene from dilute wastewater streams using titania as a photocatalyst. Sep. Purif. Technol. 28, 87–102. http://dx.doi.org/10.1016/S1383-5866(02)00017-5.

Liu, L., Yang, W., Sun, W., Li, Q., Shang, J.K., 2015. Creation of Cu_2O@TiO_2 composite photocatalysts with p–n heterojunctions formed on exposed Cu_2O facets, their energy band alignment study, and their enhanced photocatalytic activity under illumination with visible light. ACS Appl. Mater. Interfaces 7, 1465–1476. http://dx.doi.org/10.1021/am505861c.

Liu, S., Huang, J., Cao, L., Li, J., Ouyang, H., Tao, X., Liu, C., 2014. One-pot synthesis of TiO_2–WO_3 composite nanocrystallites with improved photocatalytic properties under natural sunlight irradiation. Mater. Sci. Semicond. Process. 25, 106–111. http://dx.doi.org/10.1016/j.mssp.2013.09.021.

Liu, X., Zhang, H., Liu, C., Chen, J., Li, G., An, T., Wong, P.K., Zhao, H., 2014. UV and visible light photoelectrocatalytic bactericidal performance of 100% 111 faceted rutile TiO_2 photoanode. Catal. Today 224, 77–82. http://dx.doi.org/10.1016/j.cattod.2013.09.041.

Liu, X.M., Wu, S.L., Chu, P.K., Zheng, J., Li, S.L., 2006. Characteristics of nano Ti-doped SnO_2 powders prepared by sol–gel method. Mater. Sci. Eng., A 426, 274–277. http://dx.doi.org/10.1016/j.msea.2006.04.032.

Luevano-Hipolito, E., Martinez-de la Cruz, A., Lopez-Cuellar, E., Yu, Q.L., Brouwers, H.J.H., 2014. Synthesis, characterization and photocatalytic activity of WO_3/TiO_2 for NO removal under UV and visible light irradiation. Mater. Chem. Phys. 148, 208–213. http://dx.doi.org/10.1016/j.matchemphys.2014.07.034.

Ma, J., Wu, H., Liu, Y., He, H., 2014. Photocatalytic removal of NOx over visible light responsive oxygen-deficient TiO_2. J. Phys. Chem. C 118, 7434–7441. http://dx.doi.org/10.1021/jp500116n.

Mahmoud, S.A., Yassitepe, E., Shah, S.I., 2012. Photolysis and photocatalysis of 1,4 dichlorobenzene using sputtered TiO_2 thin films. Mater. Sci. Forum 734, 215–225. http://dx.doi.org/10.4028/www.scientific.net/MSF.734.215.

Mao, C., Zuo, F., Hou, Y., Bu, X., Feng, P., 2014. In situ preparation of a Ti^{3+} self-doped TiO_2 film with enhanced activity as photoanode by N_2H_4 reduction. Angew. Chemie – Int. Ed. 53, 10485–10489. http://dx.doi.org/10.1002/anie.201406017.

Mao, D., He, F., Zhao, P., Liu, S., 2015. Enhancement of resistance to chlorine poisoning of Sn-modified MnCeLa catalysts for chlorobenzene oxidation at low temperature. RSC Adv. 5, 10040–10047. http://dx.doi.org/10.1039/C4RA15059G.

Mote, V., Purushotham, Y., Dole, B., 2012. Williamson-Hall analysis in estimation of lattice strain in nanometer-sized ZnO particles. J. Theor. Appl. Phys. 6, 6. http://dx.doi.org/10.1186/2251-7235-6-6.

Ren, R., Wen, Z., Cui, S., Hou, Y., Guo, X., Chen, J., 2015. Controllable synthesis and tunable photocatalytic properties of Ti^{3+}-doped TiO_2. Sci. Rep. 5, 10714. http://dx.doi.org/10.1038/srep10714.

Riboni, F., Bettini, L.G., Bahnemann, D.W., Selli, E., 2013. WO_3–TiO_2 vs. TiO_2 photocatalysts: effect of the W precursor and amount on the photocatalytic activity of mixed oxides. Catal. Today 209, 28–34. http://dx.doi.org/10.1016/j.cattod.2013.01.008.

Sabar, S., Nawi, M.A., Ngah, W.S.W., 2015. Photocatalytic removal of reactive Red 4 dye by immobilised layer-by-layer TiO_2/cross-linked chitosan derivatives system. Desalin. Water Treat. 3994, 1–7. http://dx.doi.org/10.1080/19443994.2015.1004113.

Sasikala, R., Shirole, A., Sudarsan, V., Sakuntala, T., Sudakar, C., Naik, R., Bharadwaj, S.R., 2009. Highly dispersed phase of SnO_2 on TiO_2 nanoparticles synthesized by polyol-mediated route: photocatalytic activity for hydrogen generation. Int. J. Hydrogen Energy 34, 3621–3630. http://dx.doi.org/10.1016/j.ijhydene.2009.02.085.

Sekiya, T., Ichimura, K., Igarashi, M., Kurita, S., 2000. Absorption spectra of anatase TiO_2 single crystals heat-treated under oxygen atmosphere. J. Phys. Chem. Solids. http://dx.doi.org/10.1016/S0022-3697(99)00424-2.

Song, K., Kwon, Y., Choi, G., Lee, W., 1999. Photocatalytic activity of Cu/TiO_2 with oxidation state of surface-loaded copper. Bull. Korean Chem. Soc. 20, 957–960.

Stefanov, B.I., Niklasson, G.A., Granqvist, C.G., Österlund, L., 2016. Gas-phase photocatalytic activity of sputter-deposited anatase TiO_2 films: effect of (001) preferential orientation, surface temperature and humidity. J. Catal. 335, 187–196. http://dx.doi.org/10.1016/j.jcat.2015.12.002.

Sun, C.Q., 2003. Oxidation electronics: bond–band–barrier correlation and its applications. Prog. Mater Sci. 48, 521–685. http://dx.doi.org/10.1016/S0079-6425(03)00010-0.

Tada, H., Kokubu, A., Iwasaki, M., Ito, S., 2004. Deactivation of the TiO_2 photocatalyst by coupling with WO_3 and the electrochemically assisted high photocatalytic activity of WO_3. Langmuir 20, 4665–4670.

Tae Kwon, Y., Yong Song, K., In Lee, W., Jin Choi, G., Rag Do, Y., 2000. Photocatalytic behavior of WO_3-loaded TiO_2 in an oxidation reaction. J. Catal. 191, 192–199. http://dx.doi.org/10.1006/jcat.1999.2776.

Wang, C., Zhang, X., Yuan, B., Wang, Y., Sun, P., Wang, D., Wei, Y., Liu, Y., 2014. Multi-heterojunction photocatalysts based on WO_3 nanorods: structural design and optimization for enhanced photocatalytic activity under visible light. Chem. Eng. J. 237, 29–37. http://dx.doi.org/10.1016/j.cej.2013.10.003.

Wang, J., Fan, H.Q., Yu, H.W., 2015. Synthesis of monodisperse walnut-like SnO_2 spheres and their photocatalytic performances. J. Nanomater. 2015. http://dx.doi.org/10.1155/2015/395483.

Wang, W., Ku, Y., 2007. Effect of solution pH on the adsorption and photocatalytic reaction behaviors of dyes using TiO_2 and Nafion-coated TiO_2 302, 261–268.

Whang, C.M., Kim, J.G., Hwang, H.J., 2005. Photocatalytic properties of the transition metal doped TiO_2 powder prepared by sol-gel process. Key Eng. Mater. 280–283, 647–650. http://dx.doi.org/10.4028/www.scientific.net/KEM.280-283.647.

Wu, X., Yu, H., Weng, D., Liu, S., Fan, J., 2013. Synergistic effect between MnO and CeO_2 in the physical mixture: electronic interaction and NO oxidation activity. J. Rare Earths 31, 1141–1147. http://dx.doi.org/10.1016/S1002-0721(12)60418-9.

Xie, Y.P., Liu, G., Yin, L., Cheng, H.M., 2012. Crystal facet-dependent photocatalytic oxidation and reduction reactivity of monoclinic WO_3 for solar energy conversion. J. Mater. Chem. 22, 6746. http://dx.doi.org/10.1039/c2jm16178h.

Yan, J., Wu, G., Guan, N., Li, L., Li, Z., Cao, X., 2013. Understanding the effect of surface/bulk defects on the photocatalytic activity of TiO_2: anatase versus rutile. Phys. Chem. Chem. Phys. 15, 10978–10988. http://dx.doi.org/10.1039/c3cp50927c.

Yang, G., Yan, Z., Xiao, T., 2012. Preparation and characterization of SnO_2/ZnO/TiO_2 composite semiconductor with enhanced photocatalytic activity. Appl. Surf. Sci. 258, 8704–8712. http://dx.doi.org/10.1016/j.apsusc.2012.05.078.

Yu, J., Wang, Y., Xiao, W., 2013. Enhanced photoelectrocatalytic performance of SnO_2/TiO_2 rutile composite films. J. Mater. Chem. A 1, 10727. http://dx.doi.org/10.1039/c3ta12218b.

Zhang, G., Xie, C., Zhang, S., Zhang, S., Xiong, Y., 2014. Defect Chemistry of the metal cation defects in the p- and n-doped SnO_2 nanocrystalline films. J. Phys. Chem. C 118, 18097–18109.

Zhang, L., Li, Y., Zhang, Q., Wang, H., 2013. Hierarchical nanostructure of WO_3 nanorods on TiO_2 nanofibers and the enhanced visible light photocatalytic activity for degradation of organic pollutants. CrystEngComm 15, 5986. http://dx.doi.org/10.1039/c3ce40620b.

Zhang, X., Ji, G., Liu, Y., Zhou, X., Zhu, Y., Shi, D., Zhang, P., Cao, X., Wang, B., 2015. The role of Sn in enhancing the visible-light photocatalytic activity of hollow hierarchical microspheres of the Bi/BiOBr heterojunction. Phys. Chem. Chem. Phys. 17, 8078–8086. http://dx.doi.org/10.1039/C5CP00184F.

Zhang, X., Qin, J., Xue, Y., Yu, P., Zhang, B., Wang, L., Liu, R., 2014. Effect of aspect ratio and surface defects on the photocatalytic activity of ZnO nanorods. Sci. Rep. 4, 4596. http://dx.doi.org/10.1038/srep04596.

Zhao, W., Zhang, M., Ai, Z., Yang, Y., Xi, H., Shi, Q., Xu, X., Shi, H., 2014. Synthesis, characterization, and photocatalytic properties of SnO_2/Rutile TiO_2/Anatase TiO_2 heterojunctions modified by Pt. J. Phys. Chem. C 118, 23117–23125.

Zheng, Z., Huang, B., Lu, J., Wang, Z., Qin, X., Zhang, X., Dai, Y., Whangbo, M.H., 2012. Hydrogenated titania: synergy of surface modification and morphology improvement for enhanced photocatalytic activity. Chem. Commun. 48, 5733. http://dx.doi.org/10.1039/c2cc32220j.

Zhou, W., Li, W., Wang, J.Q., Qu, Y., Yang, Y., Xie, Y., Zhang, K., Wang, L., Fu, H., Zhao, D., 2014. Ordered mesoporous black TiO_2 as highly efficient hydrogen evolution photocatalyst. J. Am. Chem. Soc. 136, 9280–9283. http://dx.doi.org/10.1021/ja504802q.